Applied Thermal Engineering 105 (2016) 490–500

Contents lists available at ScienceDirect

Applied Thermal Engineering

journal homepage: www.elsevier.com/locate/apthermeng

Research Paper

Evolutionary design of a satellite thermal control system: Real experiments for a CubeSat mission

Emanuel Escobar [a], Marcos Diaz [b], Juan Cristóbal Zagal [c,*]

[a] Satellite Operations Squadron, Chilean Air Force, El Bosque Air Force Base, Santiago, Chile
[b] Department of Electrical Engineering, University of Chile, Av. Tupper 2007, Santiago 8370448, Chile
[c] Department of Mechanical Engineering, University of Chile, Av. Beauchef 850, Santiago 8370448, Chile

HIGHLIGHTS

- GAs applied to automate design of CubeSat passive thermal control system (coating).
- Simulation adapted with real physical data (mockup experiment in vacuum chamber).
- Obtained coating patterns consistently outperform engineered solutions (by 5 K).
- Evolved coating patterns are far superior (by 8 K) than unpainted aluminum.

ARTICLE INFO

Article history:
Received 26 December 2015
Accepted 4 March 2016
Available online 25 March 2016

Keywords:
CubeSat
Satellite thermal control
Evolutionary design
Passive thermal control

ABSTRACT

This paper studies the use of artificial evolution to automate the design of a satellite passive thermal control system. This type of adaptation often requires the use of computer simulations to evaluate fitness of a large number of candidate solutions. Simulations are required to be expedient and accurate so that solutions can be successfully transferred to reality. We explore a design process that involves three steps. On a first step candidate solutions (implemented as surface paint tiling patterns) are tested using a FEM model and ranked according to their quality to meet mission temperature requirements. On a second step the best individual is implemented as a real physical satellite mockup and tested inside a vacuum chamber, having light sources imitating the effect of solar light. On a third step the simulation model is adapted with data obtained during the real evaluation. These updated models can be further employed for continuing genetic search. Current differences between our simulation and our real physical setup are in the order of 1.45 K mean squared error for faces pointing toward the light source and 2.4 K mean squared errors for shadowed faces. We found that evolved tiling patterns can be 5 K below engineered patterns and 8 K below using unpainted aluminum satellite surfaces.

1. Introduction

Genetic Algorithms (GA) are a form of stochastic optimization that involves intensive evaluation of candidate solutions (in the order of hundreds or thousands evaluations). This often restricts their domain of applications to problems that can be either represented by equational models or by time-saving computer simulations. GAs are starting to be applied to automate the design of satellite subsystems. In [1,2] GAs were proposed for the problem of satellite component placement or Satellite-Module Layout Design (SMLD). Evolutionary techniques such as Artificial Embryogeny [3] and Genetic Multi-Objective Optimization [4] have been recently proposed to address this challenging design problem as well.

SMLD is an example of a complex combinatorial problem in which GA are well suited due to their capacity to broadly search for solutions in highly nonlinear search landscapes. However it is also an example of a problem where representative computer simulations can be rapidly used to assess the performance of candidate solutions. Simulating a candidate module layout design simply requires a graphical verification of modules, their spaces, geometries and interference situations. This requires a reduced computing power and it is therefore convenient in the context of genetic search.

The experience shows that when applying GA to a particular design problem one should consider both, the intrinsic complexity of the target problem to be solved as well as the computational

* Corresponding author. Tel./fax: +56 22 978 4545.
E-mail address: jczagal@ing.uchile.cl (J.C. Zagal).

http://dx.doi.org/10.1016/j.applthermaleng.2016.03.024
1359-4311/

Nomenclature

ε_k	the emissivity factor
A_k	surface area of tile k
σ	Stefan–Boltzmann constant
$Q_{absorbed}$	heat incident to satellite surface (W)
$Q_{emitted}$	emitted heat from satellite surface (W)
$Q_{power\text{-}generated}$	radiation generated by the onboard electronics (W)
G_{DS}	solar constant (W/m^2)
G_{IR}	earth IR (W/m^2)
α	absorption of each material
γ	angle between an imaginary ray linking the sun and the satellite
a	Albedo factor
vf	view factor
A_{SD}	area pointing toward the sun (m^2)
A_E	area pointing toward the earth (m^2)
A_{out}	area pointing toward the space (m^2)
T	temperature (K)
q_0	energy flux (W/m^2)
q_s	contribution of a highly conductive thin shell in contact with the surface (W/m^2)
h	heat transfer coefficient used for modeling low thermal conductivity between thin shell and the surface
q_r	heat transfer due to radiation (W/m^2)
G	surface radiation from the faces to the environment (W/m^2)
C_p	heat capacity for each material (J/kg K)
ρ	density (m^3/kg)
k	thermal conductivity (W/m K)
v	variables en el dominio de búsqueda V
V	search domain for simulation
P_{lamp}	lamp power (W)
$A_{vc\_BasePlate}$	area of the vacuum chamber portion perpendicular to the light emission axis (m^2)

cost of the simulation to be used for testing each candidate solution [18]. We observe that most studies have been concentrated on problems of increasing intrinsic complexity but rely on simplistic computer simulations (like SMLD). In this work we want to give a step forward by exploring the use of GA on a satellite design task that is both, intrinsically complex and also requires a costly computer simulation to evaluate candidate solutions.

We focus our attention on the satellite thermal control design task. This problem is relevant to CubeSat design since engineers are often challenged with the problem of loading small satellites with expensive pieces of equipment, each having particular thermal characteristics and temperature requirements for successful operation. The right selection of materials and the proper placement of components is a problem of exponential complexity. Classical engineering methods have been exploited to provide acceptable, yet sub-optimal, solutions. Approaching optimality in material selection and component distribution is becoming a highly important, especially as the complexity of systems increases and constrains become stronger.

Evaluating the thermal behavior of a particular candidate solution involves the execution of a complex and expensive numerical simulation. These simulations often use a mesh representing the structure of the system to be simulated and proceed by numerically solving differential equations applying either finite difference time-domain (FDTD), finite element (FEM) or moments (MoM) methods as well as a set of boundary conditions of the problem. Analytical solutions can only be found for simple geometric scenarios that are not often representative of real satellite design situations.

In this work we use GA to explore combinations of surface painting materials that can be used to meet temperature requirements of a CubeSat. The idea is to find the right distribution so that all satellite sub-systems operate within their temperature range. We verify the process with temperature measurements performed on a 3U CubeSat mockup in a real physical setup. We are situating this problem in the context of our University CubeSat program [22]. The project "Satellite of the University of Chile for Aerospace Investigation (SUCHAI)" was the seed of our program in 2011. The satellite is 1U CubeSat carrying five proof of concept experiments about microgravity, space plasma and space technologies. The CubeSat is today ready and waiting launch. The University was recently granted funds to build and launch a couple of 3U CubeSats. For our next 3U satellite we foresee that 2/3 of the area of one face will be free of solar panels to allow deployment of booms of Langmuir probes and magnetometers. This setup motivates the present thermal design study.

The remainder of this paper is organized as follows: In Section 2, we describe a literature review related to satellite thermal problem. In Section 3, we describe the thermal control problem under analysis. Section 4 shows the process for the automated thermal design. In Section 5, we describe our results. Finally, Section 6 shows the conclusions of this study.

2. Related work

There are many related studies about the problem of modeling the thermal behavior of nanosatellites. The usual approach is to define a specific satellite layout (spatial disposition of components, heat emitters and materials, etc.) and then to model the thermal behavior under space representative conditions. Table 1 summarizes the methods and results obtained by different authors that have addressed nanosatellite thermal modeling problems.

In some studies thermal models have been validated with the aid of real physical experiments [6–12]. Corpino et al. [6] proposes finite differences for modeling the thermal behavior of LEO orbit satellites. They compared results with those obtained using ESATAN-TMS modeling software. Diaz-Aguado et al. [7] studied the thermal design of FASTRAC nanosatellite under vacuum conditions. Results were compared with those obtained using FEM. Bulut and Sozbir [8] analyzed the thermal behavior of a CubeSat using FEM. They tested different solar panel configurations. However, to the best of our knowledge there are no previous methods to automate the design of a CubeSat thermal control system using evolutionary computation, in particular for passive thermal systems.

3. Satellite thermal control problem

The purpose of a thermal control system is to maintain each satellite component within its nominal temperature limits over the entire lifespan of a satellite mission. This is especially important as we consider that in space, satellites are exposed to harsh conditions that can lead to catastrophic failures.

Table 1
Summary of related work.

Autors (year)	Method	Results
Corpino et al. [6]	Used a Finite Difference Method to simulate the thermal behavior on the PICPot nanosatellite. The results were compared with a simulation on ESATAN-TMS	The comparison between both methods showed a difference lower than 9% in the resulting battery temperature
Bulut and Sozbir [8]	Analysis of a thermal behavior of a CubeSat using Finite Difference Method. This study considers different proportions of solar cell and painted aluminum on CubeSat faces	Results showed an increase of 12 °C when using black paint coating over 7% of a structure that was initially covered with 60% solar cells and 40% aluminum sheets
Reiss [10]	Proposes an algorithm based on the use of equivalent resistances for modeling the thermal behavior of CubeSats	Results were compared with an analysis performed on ESATAN-TM software. The same distribution of temperature components was obtained when using both methods
Richmond [11]	A software tool (ATMA) was developed using a technique of equivalent resistances. The tool was intended for modeling the thermal behavior of low cost satellite systems. The software was used for assessing the performance of the CASTOR satellite	The ATMT tool was validated using the Thermal Desktop software. The results of the analysis on a solid rectangle of aluminum 6061 T6 showed a difference lower than 5% in surface temperature
Diaz-Aguado et al. [7]	In this study FEM (ABAQUS-Matlab) was used to assess the thermal behavior of FASTRC nanosatellite. A thermal cycle test (TCT) was performed on the real satellite to prove its robustness under space simulated environments, and verify the thermal design	The computational models predicted a temperature behavior that was roughly consistent with experimental data. Predicted temperatures averaged 10 °C below real measured temperatures
Lyon [12]	In this study a finite differences model is used to estimate the temperature on the faces of the FalconSat-2 satellite. The model takes into account the interaction between various internal components	The methodology allows obtaining temperature profiles as function of time for different components. The study does not consider any validation on real platform
Garzon [21]	This study is concentrated on a COMSOL implementation of FEM for analyzing the thermal behavior of OSIRIS-3U CubeSat. The study considers the theoretical effect of using thermoelectric generators (TEG) for obtaining electrical energy onboard the satellite	Results from the thermal analysis were used as a basis for the thermal design of the OSIRIS-3U CubeSat. The study also shows that using TEG will result in extremely low efficiency levels (less than 1%) due to the low temperature gradients existing on the satellite

Designers are challenged, especially within the paradigm of nano-satellites, with the problem of integrating many subsystems under a small volume. Each one having its own thermal footprint and range of operating temperatures. Due to the space constraints of CubeSat missions, engineers are not allowed to implement active control systems such as heaters, louvers and heat pipes. Instead, passive systems like surface finishes and radiators are the choice [13].

From a thermal point of view, the main challenge is to cope with the strong temperature variation between the direct sun-light and eclipse phases (from 100 °C to −130 °C in a tenth of second). In case of a LEO-orbit, the impact of this variation is extreme, since the frequency between direct sun-light and eclipse phase is very high (see Fig. 1a).

There are two critical phases for this type of orbit: These are the cold phase and the hot phase. During the cold phase, the satellite is in the eclipse zone operating to minimum power. During the hot phase, the satellite is exposed to sunlight operating to maximum power. In this paper we consider the analysis for the hot phase.

Other heat sources and sinks are important for satellite thermal balance. These are the Albedo, the Earth Infrared Radiation, the internal heat (equipment) and the heat radiated to space (see Fig. 1b).

Table 2 shows the reference values that we have used as thermal boundary conditions for this study. These values are affected by the view factor due to the angle between the light source and the faces of the satellite. This view factor is computed by the algorithm proposed by Richmond [11]. For the remainder of this paper we have considered data of two CubeSat missions: The InKlajn [14] and SUCHAI.

4. Automated thermal control design

In this section we use GA for the design of a satellite passive thermal control system. Given a temperature specification for the interior of the satellite, the idea of this process is to automatically produce a tessellation of the external faces of a satellite so that uniformly painted tiles are used to achieve a reflective surface that meets design requirements. Candidate mosaic solutions are tested under a Finite Element Method (FEM) simulation and the genetic algorithm is used to search the space of possible solutions. The painting mosaic consists on distinct squared areas covered by a uniform paint with specific thermal reflective characteristic.

We explore three steps that are illustrated in Fig. 2. The first step is the automated thermal design in simulation. This involves a Genetic Algorithm to search candidate designs and the use a FEM simulation to test que quality of each candidate. This step will be described in Section 4.1. The second step consists on fabrication of a satellite mock-up followed by an experimental test for performance evaluation. We will describe the fabrication process along with the setup and test made inside a vacuum chamber. This step will be explained in Section 4.2. The final step consists on updating the initial FEM model with real data obtained from the test.

4.1. Automated thermal design in simulation

Our method serves to automate the design of a satellite passive thermal control system. This is achieved by using genetic search in combination with a FEM simulation model that serves to assess the quality of candidate thermal control design solutions.

4.1.1. Genetic search

In this section we describe the process for automatically deriving the surface tessellation, so as to meet thermal mission requirements. The method allows choosing the paint as well as the geometric distribution of uniformly painted surface tiles. The result is interpreted as the passive thermal control law to be applied during the entire satellite mission.

A simple Genetic Algorithm [16] is used to search the space of possible solutions. We implement a three-unit (3U) CubeSat thermal simulation using FEM. The simulation is used to test the quality of candidate tessellations so as to meet the desired thermal requirements.

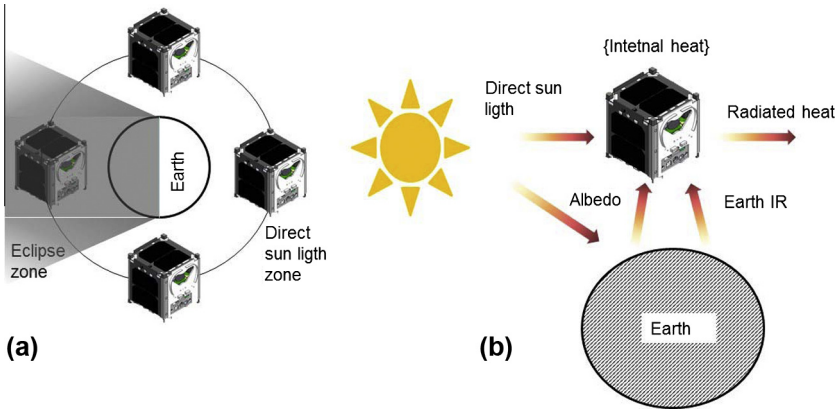

Fig. 1. Orbit phases and sources. (a) Light phases during the satellite orbit. (b) Heat contributions during operation.

Table 2
Reference values for the thermal environment.

Sources/skin	Reference value (W/m^2)	Description
Sun (solar constant)	1367	Reference value from [14,15]
Albedo	479	Fraction of solar constant, function of the view factor
Earth IR	221	Function of Earth temperature and view factor
Internal heat	20	Heat generated by the internal equipment
Radiated heat	To be computed depending on the design	

A candidate solution is represented by a 32-element length real-valued genome. Two elements are used to represent a pair of selected materials and the remaining 30 elements are used to represent the geometric distribution of material tiles over the satellite surface. As Fig. 3a illustrates, there is a total of 10 satellite faces (five on top and five at the bottom) under genetic optimization. The central portion of the satellite consists of fixed solar panels.

A tile is a rectangular region occupying a percentage of a face surface. Fig. 3c shows how the geometry is defined by three surface factor coefficients in the range [0,1]. Fig. 3a illustrates a solution with two different materials shown with varying shades of green[1]. Table 5 shows the properties of the four materials that were considered for optimization. A representation of the genome codified it shown in Fig. 3b.

An initial population of 12 candidate solutions was first randomly generated. Then the algorithm proceeds as follows: The fitness of each candidate solution is evaluated using the thermal simulation. Parents for a new generation are selected using stochastic universal sampling (SUS) [17,18]. Crossover is performed with a probability Pc = 0.8 and mutation with a probability Pm = 0.03 per gen. The process repeats for each new generation until a total of one hundred generations have been evaluated.

The fitness function was selected to be a measure of the total product between patch emissivity and local temperature, the idea behind this approach is to maximize the amount of heat dissipated by the satellite. This function is shown in Eq. (1)

$$Fitness = \sigma \cdot \sum_{k=1}^{N} \left(\varepsilon_k \cdot \int_{A_k} t \cdot dA \right) \quad (1)$$

[1] For interpretation of color in Fig. 3, the reader is referred to the web version of this article.

where $N = 40$ is the total number of tiles under optimization, A_k [m^2] is the area of a radiating tile k, ε_k is the emissivity factor of tile k and σ [$W/m^2 K^4$] is the Stefan–Boltzmann constant.

4.1.2. Thermal analysis

The satellite thermal behavior can be analyzed following the relations of sources and sinks of heat shown in Fig. 1b. The heat contributions are summarized in Eq. (2).

$$Q_{absorbed} - Q_{emitted} + Q_{power\text{-}generated} = 0 \quad (2)$$

where

$$Q_{absorbed} = G_{DS} \cdot A_{DS} \cdot \alpha \cdot \cos(\gamma) + G_{DS} \cdot A_E \cdot a \cdot \alpha \cdot vf + G_{IR} \cdot A_E \cdot vf \quad (3)$$

$$Q_{emitted} = A_{out} \cdot \varepsilon \cdot \sigma \cdot T^4, \quad (4)$$

The parameters included in Eqs. (3) and (4) are summarized in Table 3.

The power $Q_{power\text{-}generated}$ is generated by the onboard electronics, such as batteries, controller, GPS, transceiver, computer and the payloads (e.g. camera). Although, these values are different for each satellite, the standard values used in this paper are summarized in Table 4. For simulation purposes we assume that the thermal loads are homogenously distributed on the internal wall of the satellite.

The pool of paint materials to be used during evolution is shown in Table 5. We selected this list of materials according to their absorption–emission coefficients, their local marked availability and reported NASA recommendations as common spacecraft thermal-control coatings [13,20].

Finally, the thermal analysis is computed using FEM. This analysis allows simulating the temperature distribution on the satellite for all the created configurations (see Fig. 2, step 1).

4.2. FEM model

A FEM model is used to assess the quality of each candidate mosaic solution by making explicit the resulting satellite surface temperature distribution. The model is used each time that a new individual requires to be evaluated during evolution. Therefore, it is critical for the model to be computationally efficient. A time consuming model will slow down the optimization process while a rapid but inaccurate model would result in fruitless results.

The model uses the geometry of a 3U CubeSat (10 cm × 10 cm × 30 cm) with 40 rectangular tiles of varying geometry defined by the surface factors of each individual genome.

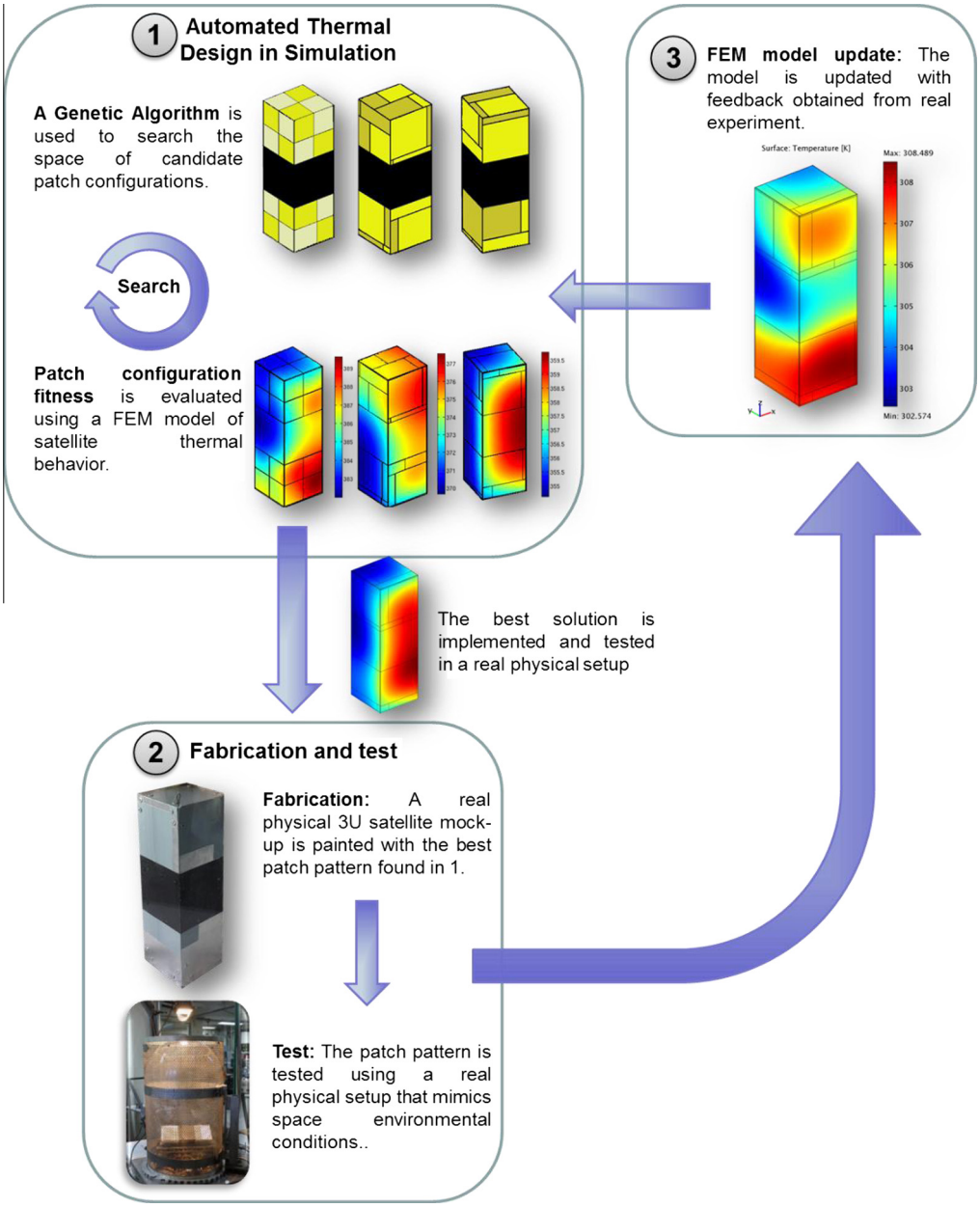

Fig. 2. Scheme of the three steps explored on this paper. Step 1 is the automated thermal design in simulation. This involves using a FEM model and a Genetic Algorithm to efficiently search candidate designs. Step 2 consist on a fabrication of a satellite mock-up followed by an experimental test of resulting properties. Step 3 consists on updating the initial FEM model with real data obtained from the test.

The tile thickness is set to 1 mm. Since the middle region is used by solar panels, these are represented by uniform squared surfaces.

A computational mesh is defined with a total of 14,000 tetrahedral elements. Each element is analyzed using Comsol in terms of energy transfer according to Eq. (5) but considering steady state ($\rho C_p = 0$).

$$\rho C_p \frac{\partial T}{\partial t} + \nabla \cdot (-k\nabla T) = q_0 + q_r + q_s + h(T_{inf} + T), \tag{5}$$

For Eq. (5) q_0 represents the energy flux (W/m^2) incident normal to the satellite surface. The value used for the model is shown in Eq. (3) as $Q_{absorbed}$ and Table 3. The term q_s represents the contribution of a highly conductive thin shell in contact with the surface. This contribution is not present on the boundary conditions of the model. The term h is a heat transfer coefficient used for modeling low thermal conductivity between thin shell and the surface. In some cases it is also useful modeling the cooling process of convective effects due to the exposition of the surface to fluid flux at low temperatures T_{inf}. However, this contribution is not present in our boundary conditions since the satellite operates in vacuum and therefore we neglect the convective term. The term q_r represents the heat transfer due to radiation, which is expressed by Eq. (6).

$$q_r = \varepsilon(G - \sigma T^4), \tag{6}$$

where the term G represents a surface radiation from the faces to the environment in the case of the external faces of the CubeSat or irradiation toward neighboring surfaces in the case of internal faces of the satellite. The constant $C_p = 936$ [J/kg K] and $k = 150$ [W/m K]. These values correspond aluminum 6061 [15].

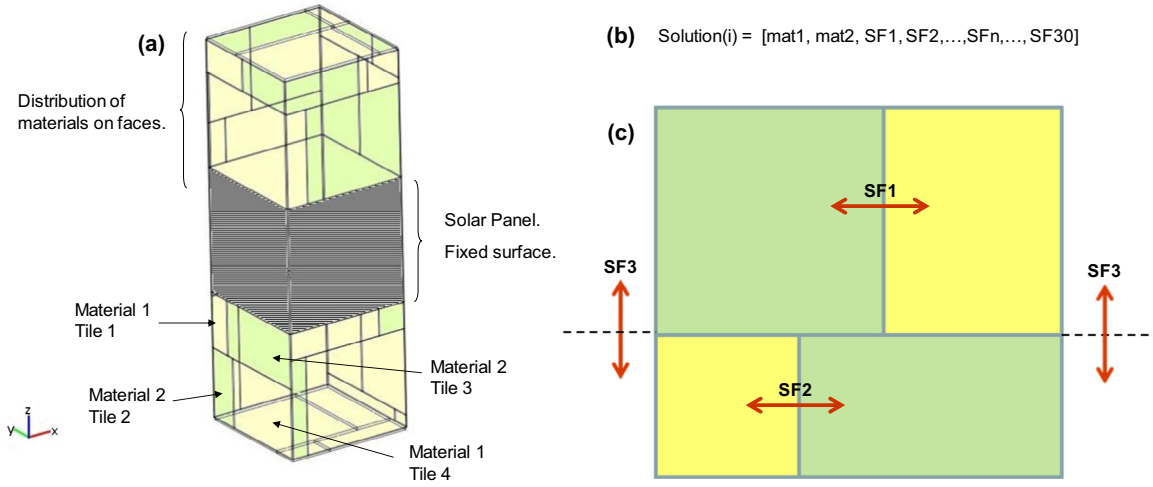

Fig. 3. Example of thermal control material solution, scheme of the genome for the solutions and configuration of one face using the Surface Factors. (a) Distribution of material tiles on faces model. Each face contains four tiles of two different materials. (b) Scheme that show the codification of the genome for each solution. The two first genes represent the used materials, the remaining thirty represent the Surface Factors. (c) Distribution of patches on one face defined by a combination of three Surface Factors (SF).

Table 3
Parameters used for thermal analysis [14,19].

Parameter	Description	Value
G_{DS}	Solar constant	1367 (W/m^2)
G_{IR}	Infrared radiation, which is a function of the Earth temperature and view factor	221 (W/m^2)
α	Absorption of each material	See Table 5
ε	Emission coefficient of each material	See Table 5
γ	Angle between an imaginary ray linking the sun and the satellite, versus a vector normal to the face receiving direct sun light. One value is required for each face	$\left[\frac{\pi}{2}, \frac{3\pi}{4}, \frac{3\pi}{4}, \frac{\pi}{4}, \frac{\pi}{4}, \frac{\pi}{2}\right]$
a	Albedo factor	35%
vf	View factor [9,11]. Six values were used	[0.24, 0.6, 0.6, 0.02, 0.02, 0.24]
σ	Stephan–Boltzmann constant	5.67e−8 (W/m^2 K^4)
A_{SD}, A_E, A_{out}	Areas pointing toward the sun, earth and space respectively	Defined by patch parameters
T	Temperature	To be computed

Table 4
Nominal power generated by on board electronic components [14]. These values were used for the generation of the FEM model and the optimization process used on step 1.

Component	Day (W)	Night (W)
Alinco	1.92	1.92
PicoPacket	6.00E−02	6.00E−02
ATOMIC CLOCK	7.5	0
GPS	1.2	0
ABSL BATERY	0.1	0.3
MGT	0.3	1.5
MCU-2	1.00E−01	1.00E−01
ISIS TXRX	3.24	3.24
PDU	0.25	0.25
EPS-2	1.63	0.37
EPS-1	1.63	0.37
MCU-1	1.00E−01	1.00E−01
ARAZIM MGM	0.132	0.0055
GYRO	0.5	0.5
Total	18.662	8.7155

Table 5
Materials used during simulations.

ID	Material	α	ε
1	Brilliant Aluminum Paint	0.3	0.31
2	Epoxy Aluminum Paint	0.77	0.81
3	Finch Aluminum Paint	0.22	0.23
4	Leafing Aluminum Paint	0.37	0.36

4.3. Experimental setup

We carried real thermal experiments using a 3U at-scale CubeSat mock-up. Our tests aimed at reproducing the surrounding space and internal satellite environmental thermal conditions that arise when a satellite is directly illuminated by the sun. We took special attention at reproducing the illumination and vacuum conditions as best as possible. The mock-up was constructed using 1 mm thickness aluminum sheets that were folded into a 3U CubeSat resembling shape. The sheets were held together using POP rivets. The mockup external surfaces were painted following the covering pattern that resulted from the automated design stage performed with the aid of a FEM simulation (see Fig. 2, step 1).

The painted mockup is displayed in Fig. 4a. A total of 64 NTC thermistors were distributed on the internal faces of the mockup. Fig. 4b shows the internal distribution of sensors (13 on each lateral face, 5 on top and 5 on the bottom face). The sensors were held in place with Kapton film as shown in Fig. 4c. Small pieces of circuitry were placed inside the mockup, all of them displaying a negligible heat-emitting footprint. Cables were routed outside the mockup and data was acquired thanks to the use of an Arduino Uno and nine multiplexer units (8-channel analog multiplexer 74HC4051). The multiplexers served at expanding the amount of readable inputs from six up to 72. We followed the thermistor calibration procedure suggested by the manufacturer (NTC MF58Z) resulting in a ±0.6 °C measurement error.

To prevent convective transport of heat and to accurately mimic space conditions we placed the mockup inside a high vacuum chamber (Veeco Instruments series 775, 40 cm diameter) that maintained a low pressure level of 5.4E−6 mbar during the complete test. This pressure level is a good approximation to what can be observed on low orbits [13,15]. The chamber consisted on a 1 cm thickness transparent glass bell with a stainless steel

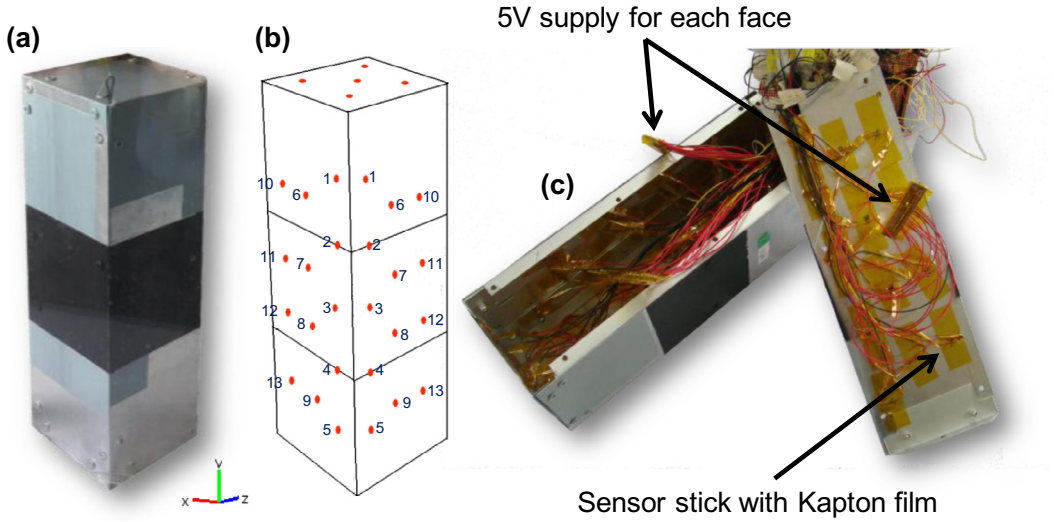

Fig. 4. Sensorized mock-up of 3U CubeSat. (a) Aluminum mock-up painted with the genetically evolved pattern that resulted on step 1. (b) Spatial disposition of temperature sensors inside mock-up (64 NTC thermistors). Blue numbers represent the position on each lateral face. Thirteen sensors were placed on each lateral face. Five sensors on top and five sensors on bottom faces, respectively. (c) Sensors attached with Kapton film. (For interpretation of the references to color in this figure legend, the reader is referred to the web version of this article.)

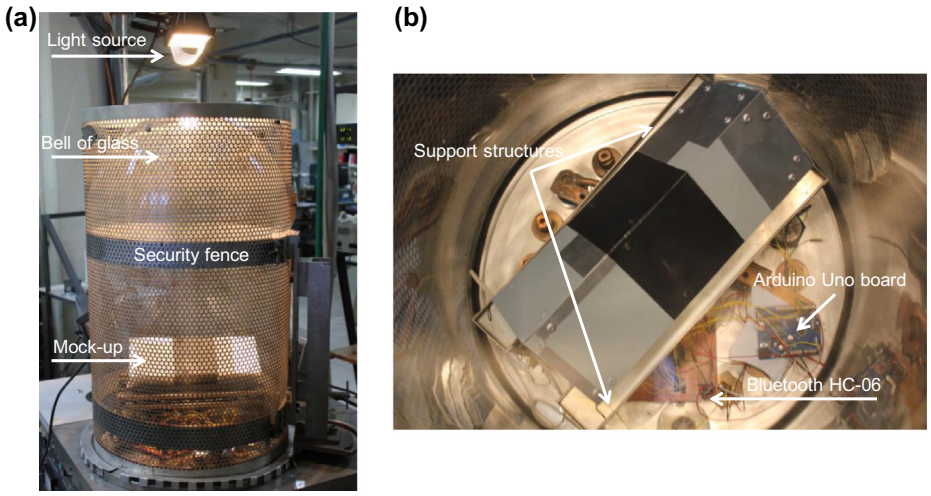

Fig. 5. Experimental setup. (a) View of the mock-up inside of the vacuum chamber. The light source is on top of the chamber, the vacuum chamber and the mock-up inside of the chamber. (b) Mock-up inside of the vacuum chamber. This figure shown the structures that support the mock-up, the Arduino Uno board and the Bluetooth HC-06 which sent the information of temperature outside of the vacuum chamber.

support. The chamber was surrounded by a cylindrical mesh guard made of carbon steel. The guard was open on top avoiding interference with the experimental light beam. Fig. 5a shows the vacuum chamber with the satellite mockup contained inside at the bottom. Fig. 5b shows details the internal disposition of mockup and measurement electronics. To prevent conductive transport of heat we supported the mockup with the help of Kapton film that served at isolating the mockup body from the bottom of the chamber. A 150 W halogen lamp was placed pointing toward the mockup, at a distance of 94 cm from the replica (see Fig. 5a). The lamp served at representing the effect of sun light. The experiment lasted until the temperature on all sensors was settled and temperatures recorded after six hours of operation.

Once the experiment was completed the data was stored for subsequent update of the FEM model. The experimental values were used to update the model following the procedure shown in Section 4.4.

4.4. FEM model update

Updating a simulation model is relevant to this study since we want to validate our results with a real experimental setup and we also want to maintain a representative model. This updated model can be used to continue evolution or to predict the behavior of the system under different circumstances. Moreover, it is known that systems evolving under simulation might have a tendency to exploit peculiarities of the model to maximize their fitness and might fail to be transferred to reality [23]. Therefore, alternatives for grounding simulation are required.

A simulation model can be automatically adjusted against a real physical setup by using the error between model predictions and real measurements as a feedback. Internal variables defining the model (such as FEM mesh size, integration steps, and constants) can be adjusted toward minimizing these differences. This type of inference-based model adaptation has been previously explored

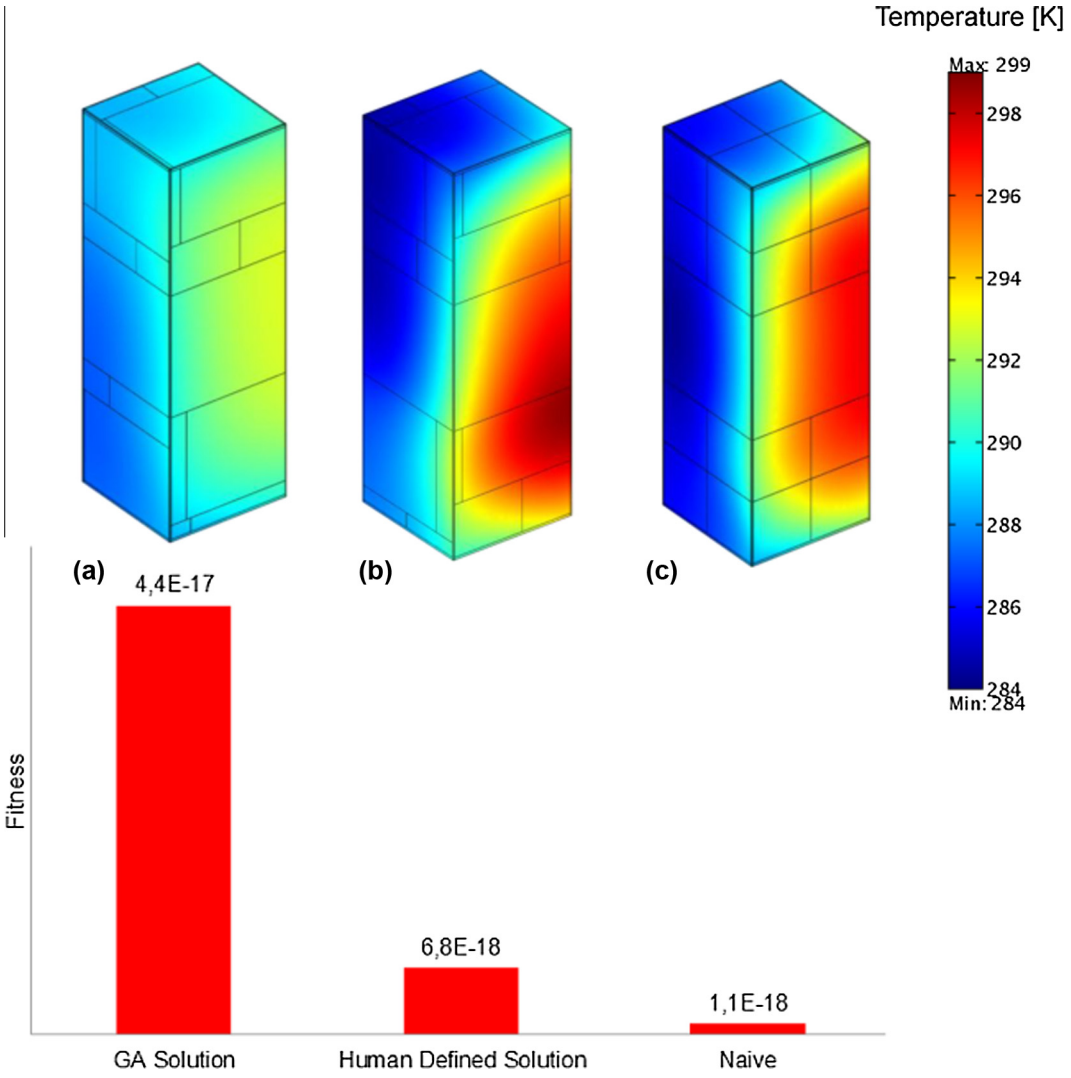

Fig. 6. Heat distributions (top images) resulting from the FEM simulation of a 3U CubeSat under sun light phase when using three different paint solutions. Sun radiation arrives from right to left. (a) Result for the solution obtained when using the GA method. (b) Result for the human-made solution. (c) Result from a trivial solution. The corresponding fitness values (see Eq. (1)) are shown at the bottom of each image. As expected, lower surface temperatures result when maximizing the fitness function.

in the context of robotics [24,25], and allows adjusting critical simulation variables without explicitly measuring them but relying on simple comparisons between model/reality outputs.

During step 2 we transferred to reality the best solution obtained in step 1 (see Fig. 2) and we measured a set of real surface temperatures T_i^R, with $i = \{1, \ldots, 64\}$. We now define a set of candidate simulation models S_v with v representing a particular set of simulation variables. As expressed in (7) there exist a set of simulation variables v in a bounded search domain V such that the differences between temperatures measured in reality T^R versus temperatures predicted by the model T^{s_v} is minimized according to certain norm.

$$\{\exists\, v \in V \,|\, \min(\|T^R - T^{s_v}\|)\} \tag{7}$$

We used this concept to adapt our simulation model with real measurements from the satellite mock-up setup. $Q_{absorbed}$ (see Eq. (3)) was chosen as the internal model variable over which inference was taken. So the set $v = \{Q_{absorbed}\}$ corresponds to a single scalar value. The initial value of this variable is described in Eq. (8) as

$$Q_{absorbed} = \frac{P_{lamp}}{A_{vc\_BasePlate}} \cos(\gamma) \tag{8}$$

where P_{lamp} is the lamp power (see Fig. 5a). $A_{vc\_BasePlate}$ is the area of the vacuum chamber portion perpendicular to the light emission axis and γ is the angle sustained by the mock-up faces pointing toward the light source (see Table 3).

We then executed a one variable search process by defining a bounded search domain $V = \{Q_{absorbed} - \delta, Q_{absorbed} + \delta\}$ with δ being equal to 10 W/m^2. Starting from the minimum value of v, the search consisted on increasing v, running the simulation with the new value until the error norm started to increase again. Despite the simplicity of this process we found a new value $Q_{absorbed\_experimental}$ that results in small discrepancies between the simulation and the real experiments. These differences will be discussed in the next section.

5. Results of optimization process

The results of the optimization process on the 3U CubeSat are shown in Fig. 6. Brilliant and Epoxy aluminum paints (Table 5, ID1, ID2) were selected by the GA. The illustration shows paint distributions obtained as result of evolution (a, GA Solution), a human-made solution (b, Human Defined Solution) and a trivial naive solution (c, Naive). The figure represents the direct sun light

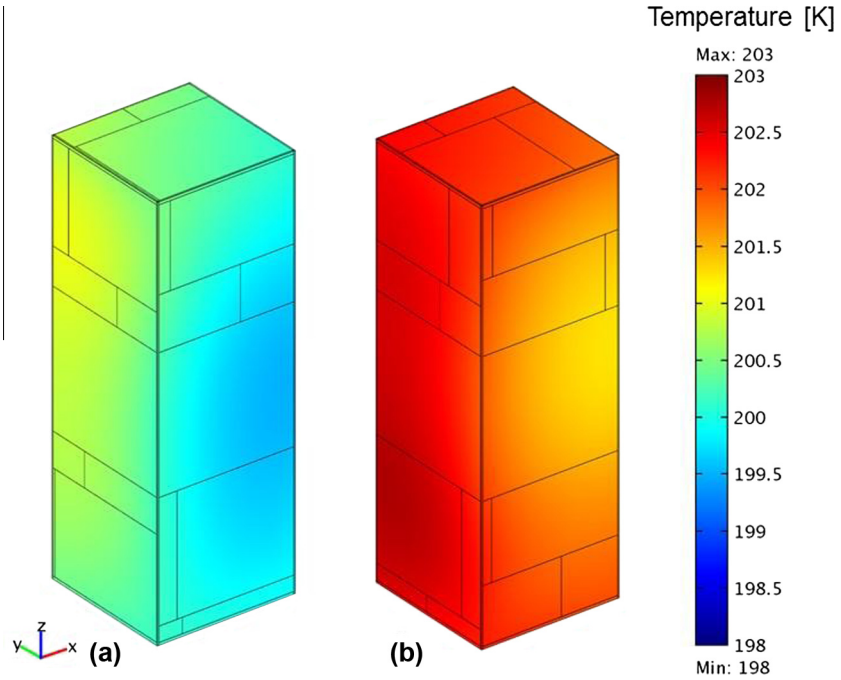

Fig. 7. Heat distributions resulting when evaluating two solutions during night time (cold-case). Earth radiation arrives from left to right. (a) Result for the solution obtained when using the GA method. (b) Result for the human-made solution. The surface temperatures of the evolved solution fall in the range of [199–201] Kelvin which is acceptable for external satellite components according to [15].

satellite phase, also known as hot-case. The sun radiation arrives from right to left. The temperature color bar is shown on top, at the right side of images. Corresponding values of fitness are presented at the bottom, below each figure.

The human-made solution was generated by a thermal engineer who manually adjusted tiles toward maximizing fitness until reaching his best. The naive solution consisted on tiles of equal size. It is possible to appreciate how different paint patterns produce alternative surface temperature distributions, affecting the energy dissipated by the thermal control system.

Since the solution was evolved to improve heat dissipation during the hot-case we also wanted to verify the behavior during the cold-case (eclipse zone) and corroborate whether satellite temperatures remain under an acceptable range. During night time the heat emission might increase leaving satellite components below their operational values. Fig. 7 shows heat distributions resulting when evaluating two solutions during night time (cold-case). Earth radiation arrives from left to right on this figure. The illustration shows the solution obtained when using the GA method (a, GA Solution) and results for the human-made solution (b, Human Defined Solution). The surface temperatures of the evolved solution fall in the range of [199–201] Kelvin which is acceptable for external satellite components according to [15].

Fig. 8 shows simulated temperature values at the thirteen sensorized locations defined in Section 4.3. Temperatures for the hot-case are given at each location for GA solution, human defined solution and naïve solution. One can observe how the optimized solution consistently results in lower temperatures for the case of faces pointing toward the sun (Faces 2 and 3). In some cases this results in a difference of 5 K.

5.1. Results after model update

Fig. 9 (Left) shows 3D views of a simulated best evolved solution for faces F1/F2 in (a) and faces F3/F4 in (b). The center-right portion of the figure shows comparisons between the simulated baseline condition (black triangles) where the satellite surface is left unpainted versus the evolved condition (real mock-up: blue diamonds, simulated satellite: red squares) for faces F1 (c), F2 (d), F3 (e), F4 (f).

Comparisons are shown for the temperature measurement for the thirteen points used during the real experiments (see Fig. 4b). Sensor numbers indicate the identification of each sensor marker. The position of markers is displayed in Fig. 4. These experiments indicate a clear reduction in temperature when covering surfaces with the evolved tiling pattern. One can also appreciate a high correlation between simulated and real data for the evolved condition. This correlation is especially high in the case of F3 and F2, the pair of faces that was pointing toward the light source. Faces F1 and F4 were on shadow.

One should consider that the simulation model does not takes into account the influence of the vacuum chamber protective grid that reflects some of the light energy coming from the halogen lamp. The model disregards the influence of the fixtures that are used for supporting the mockup.

Despite these simplifications one can observe a high correlation between the temperature values predicted form the model and those measured during the real experiments. The model is particularly accurate for predicting the behavior of faces pointing toward the light source (faces F2 and F3). In this case a mean squared error of $MSE_L = 1.45$ K is observed between model vs real temperatures. Less precision is observed when comparing experimental and predicted temperature values for the shadowed faces (F1 and F4). In this case a mean squared error of $MSE_S = 2.4$ K is observed between model vs real temperatures. One possible explanation for these differences is given by the presence of fixtures that carry conductive temperature transference.

This level of model accuracy is a good improvement with respect to previous work where accuracies in the range of 10 K have been observed when comparing FEM models vs real CubeSat mockup data [7].

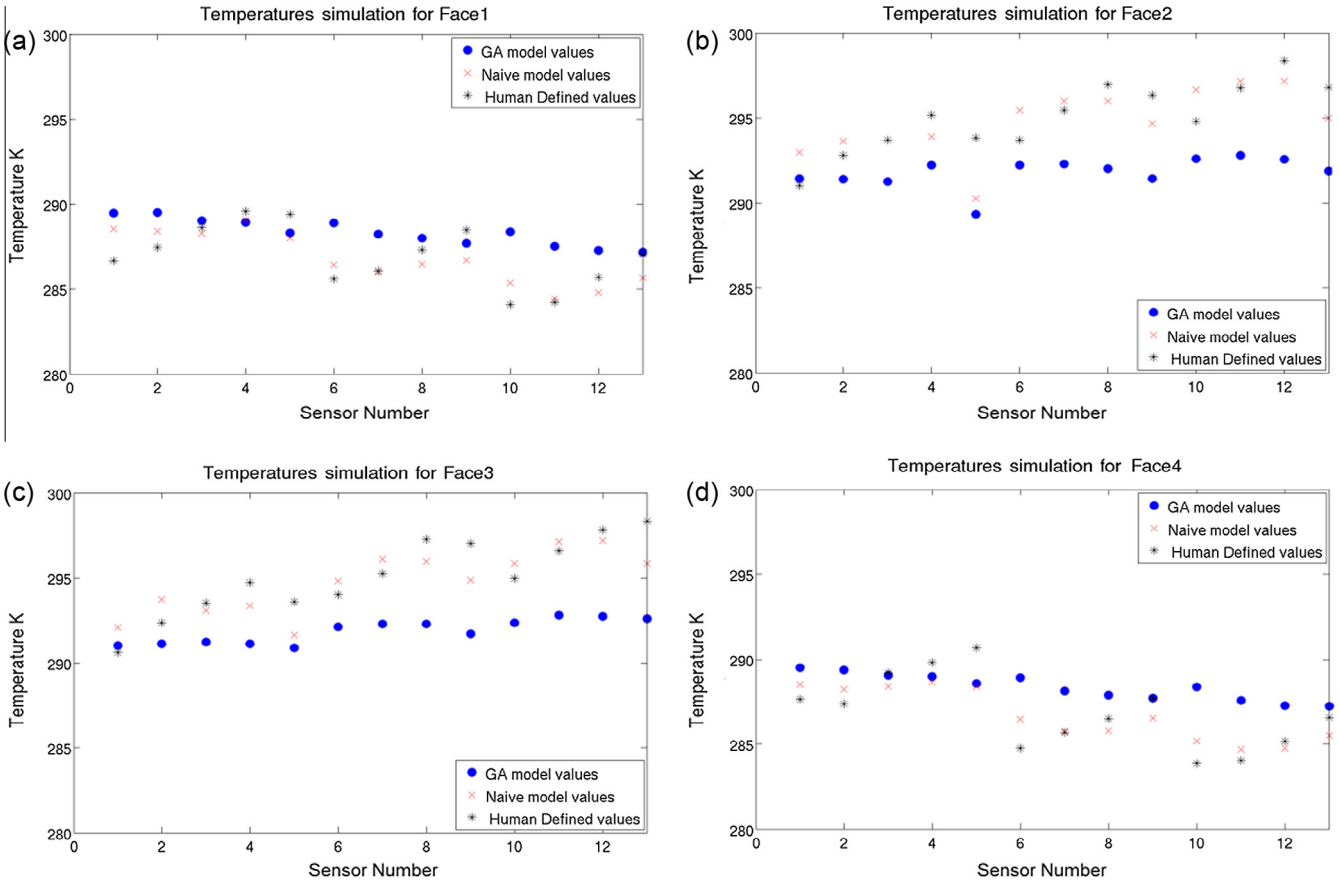

Fig. 8. Simulated temperature values at the thirteen sensorized locations defined in Section 4.3. Temperatures for the hot-case are given at each location for GA solution, human defined solution and naïve solution. One can observe how the optimized solution consistently results in lower temperatures for the case of faces pointing toward the sun (Faces 2 and 3). In some cases this results in a difference of 4 K.

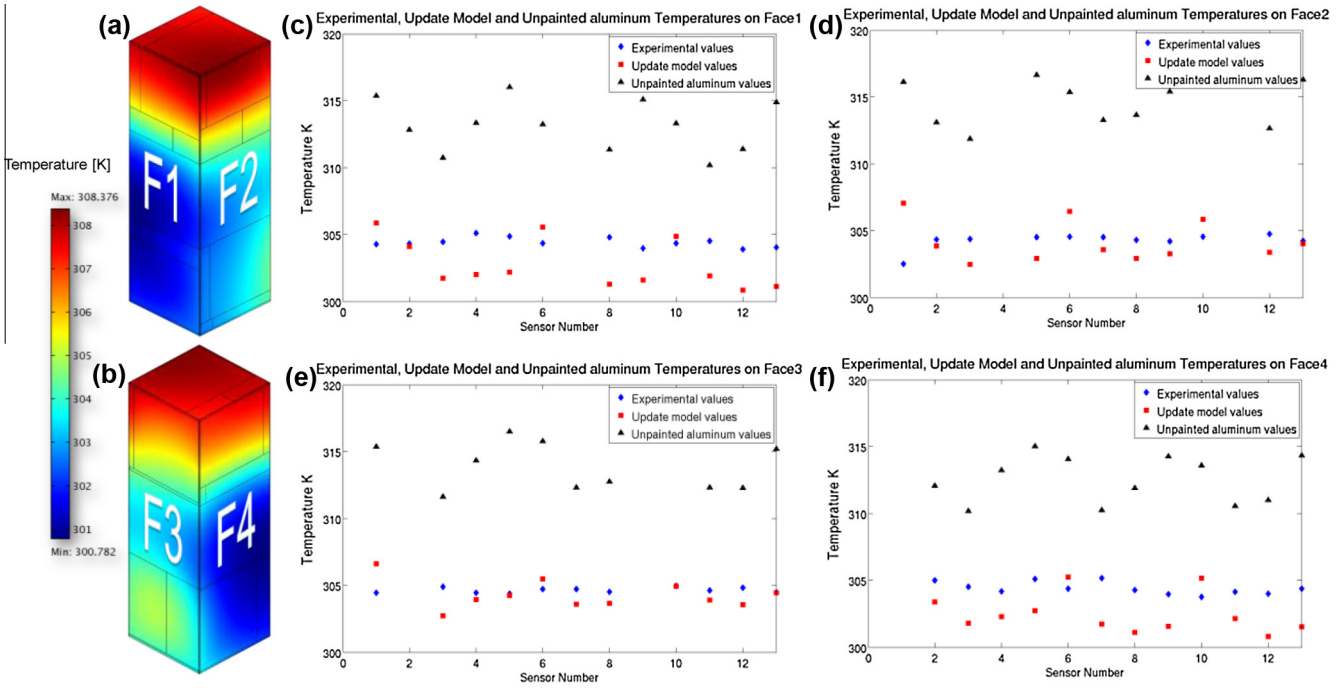

Fig. 9. Left: 3D views of a simulated best evolved solution for faces F1/F2 in (a) and faces F3/F4 in (b). Center-Right: Comparison between simulated baseline condition (black triangles) where the satellite surface is left unpainted versus evolved condition (real mock-up: blue diamonds, simulated satellite: red squares) for faces F1 (c), F2 (d), F3 (e), F4 (f). Sensor number indicates the identification of each sensor marker. The position of markers is displayed in Fig. 4. These experiments indicate a clear reduction in temperature when covering surfaces with the evolved tiling pattern. One can also appreciate a high correlation between simulated and real data for the evolved condition. This correlation is especially high in the case of F3 and F2, the pair of faces that was pointing toward the light source. (For interpretation of the references to color in this figure legend, the reader is referred to the web version of this article.)

6. Conclusions

We have presented a method to automate the design of a satellite passive thermal control system. The method uses genetic algorithms to search a space of possible candidate solutions. Each solution is evaluated using a thermal FEM simulation of a CubeSat. We tested the capability of the method on a search space defined by varying satellite surface paint tiles made with different paint materials. To validate this method, we implement a real physical satellite mockup and we tested its thermal behavior using a vacuum chamber and incandescent light source.

We summarize the main results of this work as follows:

1. We have presented a method of artificial evolution for the design of a CubeSat passive thermal control system. We explored the case of evolving tiling patterns for covering the satellite surface.
2. The evolved solution was transferred to a real physical setup for validation and model calibration purposes.
3. After calibration of the simulation model it was possible to obtain solutions with high levels of accuracy (in the order of 1.45 K mean squared errors for faces pointing toward the light source and 2.4 K mean squared errors for shadowed faces).
4. One possible explanation for discrepancies between simulation and reality is given by the presence of fixtures that allow conductive heat transference on shadowed faces.
5. Evolved tiling patterns of faces pointing toward the sun light consistently show lower temperatures compared with engineered solutions (in some cases 5 K below) and even below compared with a naïve solution (Fig. 8).
6. Covering the satellite with an evolved tiling pattern results in temperatures on the order of 8 K below the alternative of using unpainted aluminum surfaces (Fig. 9).

The satellite thermal control was evolved to maximize heat dissipation during sun light phase. We verified that the resulting design also allows various satellite components to operate during night time but some internal components might require heaters to meet operational specifications. An alternative for future implementations of the proposed methodology would be to maximize heat dissipation until the performance on the cold case remains under specifications or to explicitly incorporate the cold case behavior in the fitness function.

Finally, to illustrate the significance of the presented study we quote a recent NASA report [26] statement on today's CubeSat technology gaps: "*Nanosats are approaching a scale (6U) at which more power can be generated than can be passively dissipated with current technology. Active systems at CubeSat scale or novel passive systems are needed*". Our study shows an avenue for the automated design of novel passive systems. As the complexity of satellite systems increase it will be more difficult for engineers to analyze different design alternatives and design automation becomes important.

Acknowledgements

We thank funding provided by FONDECYT project number 1151476, Conicyt Anillo project number ACT1405 and ANR-Conicyt project number 47.

References

[1] H.F. Teng, Y. Chen, W. Zeng, Y.J. Shi, Q.H. Hu, A dual-system variable-grain cooperative coevolutionary algorithm: satellite-module layout design, IEEE Trans. Evol. Comput. 14 (3) (2010) 438–455.
[2] B. Zhang, H.F. Teng, Y.J. Shi, Layout optimization of satellite module using soft computing techniques, Appl. Soft Comput. 8 (1) (2008) 507–521.
[3] K.O. Stanley, R. Miikkulainen, A taxonomy for artificial embryogeny, Artif. Life 9 (2) (2003) 93–130.
[4] C.D. Jilla, A multiobjective, multidisciplinary design optimization methodology for the conceptual design of distributed satellite systems, PhD dissertation, Aeronautics and Astronautics, Massachusetts Institute of Technology, Cambridge, MA, 2002.
[6] S. Corpino, M. Caldera, M. Masoero, F. Nichele, N. Viola, Thermal design and analysis of a nanosatellite in low earth orbit, Acta Astronaut. 115 (2015) 247–261.
[7] M.F. Diaz-Aguado, J. Greenbaum, W.T. Fowler, E.G. Lightsey, Small satellite thermal design, test, and analysis, in: Defense and Security Symposium. International Society for Optics and Photonics, 2006.
[8] M. Bulut, N. Sozbir, Analytical investigation of a nanosatellite panel surface temperatures for different altitudes and panel combinations, Appl. Therm. Eng. 75 (2015) 1076–1083.
[9] C.B. Van Outryve, A Thermal Analysis and Design Tool for Small Spacecraft Master Thesis, San Jose State University, CA, USA, 2008.
[10] P. Reiss, New Methodologies for the Thermal Modelling of CubeSats, in: The 4S Symposium, 2012, pp. 1–16.
[11] J.A. Richmond, Adaptive Thermal Modeling Architecture for Small Satellite Applications. Aeronautics and Astronautics Master Thesis, Massachusetts Institute of Technology, Cambridge, MA, USA, 2010.
[12] C.I.C. Lyon, L.J. Sellers, C. Underwood, Small satellite thermal modeling and design at USAFA: FalconSat-2 applications, in: Aerospace Conference Proceedings, vol. 7, IEEE, 2002, pp. 7–3391.
[13] D.G. Gilmore, Spacecraft Thermal Control Handbook: Fundamental Technologies, vol. 1, AIAA, 2002.
[14] D. Rockberger, Thermal and Mechanical Optimization of the First Israeli Nano-Satellite, in: Proceeding of the 49th Israel Annual Conference on Aerospace Sciences, 2009.
[15] R.D. Karam, Satellite Thermal Control for Systems Engineers, vol. 181, AIAA, 1998.
[16] D.E Golberg, Genetic Algorithms in Search, Optimization, and Machine Learning, Addion Wesley, 1989.
[17] J.E. Baker, Reducing bias and inefficiency in the selection algorithm, in: Proceedings of the Second International Conference on Genetic Algorithms, 1987.
[18] M. Gen, R. Cheng, Genetic Algorithm and Engineering Optimization, John Wily and Sons, New York, 2000.
[19] W.J Larson, J.R Wertz, Space Mission Analysis and Design (No. DOE/NE/32145–T1), Microcosm Inc., Torrance, CA, 1992.
[20] J.H. Henninger, Solar Absorptance and Thermal Emittance of Some Common Spacecraft Thermal-Control Coatings (No. NASA-RP240400-1121), National Aeronautics and Space Administration, Washington, DC, 1984.
[21] M.M. Garzon, Development and Analysis of the Thermal Design for the OSIRIS-3U CubeSat, The Pennsylvania State University, 2012 (Doctoral dissertation).
[22] M.A. Diaz, J.C. Zagal, C. Falcon, M. Stepanova, J.A. Valdivia, M. Martinez-Ledesma, J. Diaz-Pena, F.R. Jaramillo, N. Romanova, E. Pacheco, M. Milla, M. Orchard, J. Silva, F.P. Mena, New opportunities offered by CubeSats for space research in Latin America: the SUCHAI project case, Adv. Space Res. (2016) (in press).
[23] J.C. Bongard, H. Lipson, Nonlinear system identification using coevolution of models and tests, Evol. Comput. IEEE Trans. 9 (4) (2005) 361–384.
[24] J. Bongard, V. Zykov, H. Lipson, Resilient machines through continuous self-modeling, Science 314 (5802) (2006) 1118–1121.
[25] J.C. Zagal, J. Ruiz-Del-Solar, Combining simulation and reality in evolutionary robotics, J. Intell. Rob. Syst. 50 (1) (2007) 19–39.
[26] NASA, Ames Research Center. Small Spacecraft Technology State of the Art, Moffet Field, CA, NASA/TP–2014-216648/REV1, 2014.